Role of Putative Anion-Binding Sites in Cytoplasmic and Extracellular Channels of *Natronomonas pharaonis* Halorhodopsin†

Maki Sato,‡ Megumi Kubo,‡ Tomoyasu Aizawa,‡ Naoki Kamo,§ Takashi Kikukawa,|| Katsutoshi Nitta,‡ and Makoto Demura*,‡

Division of Biological Sciences, Graduate School of Science, Hokkaido University, Sapporo 060-0810, Japan, Graduate School of Pharmaceutical Sciences, Hokkaido University, Sapporo 060-0812, Japan, and Center for Advanced Science and Technology, Hokkaido University, Sapporo 001-0021, Japan

Received November 29, 2004; Revised Manuscript Received January 27, 2005

ABSTRACT: *Natronomonas (Natronobacterium) pharaonis* halorhodopsin (NpHR) is an inward light-driven Cl^- ion pump. For efficient Cl^- transport, the existence of Cl^--binding or -interacting sites in both extracellular (EC) and cytoplasmic (CP) channels is postulated. Candidates include Arg123 and Thr126 in EC channels and Lys215 and Thr218 in CP channels. The roles played by these amino acid residues in anion binding and in the photocycle have been investigated by mutation of the amino acid residues at these positions. Anion binding was assayed by changes in circular dichroism and the shift in the absorption maximum upon addition of Cl^- to anion-free NpHR. The binding affinity was affected in mutants in which certain EC residues had been replaced; this finding revealed the importance of Arg123. On the other hand, mutants in which certain residues in the CP channel were replaced (CP mutants) did not show changes in their dissociation constants. The photocycles of these mutants were also examined, and in the case of the EC mutants, the transition to the last step was greatly delayed; on the other hand, in the CP mutants, L2-photointermediate decay was significantly prolonged, except in the case of K215Q, which lacked the O-photointermediate. The importance of Thr218 for binding of Cl^- to the CP channel was indicated by these results. On the basis of these observations, the possible anion transport mechanism of NpHR was discussed.

Halorhodopsin (HR)[1] (*1*−*5*) and bacteriorhodopsin (BR) (*6*−*8*) are transmembrane, seven-helix proteins in *Halobacterium salinarum*, and these proteins bear retinal as a chromophore. These proteins act as an inward-directed electrogenic light-driven chloride ion pump (HR) and an outward-directed proton pump (BR), respectively. Because of its high stability and abundance, BR has become a model system for studying membrane protein structure, protein folding, bioenergetics, photochemistry, and the mechanisms of proton transport (*5*, *9*−*11*). However, much less information is available regarding the molecular mechanism of Cl^- transport by HR.

Illumination of BR elicits a linear and cyclic type of photochemistry commonly termed the "photocycle". According to this process, illumination excites BR, followed by relaxation via various photointermediates to an original, unphotolyzed BR state (*12*, *13*). Photoexcitation of all-*trans*-retinal initiates the photocycle with retinal isomerization to the 13-*cis* form, and the early intermediates (K and L) are produced. In the next step, a proton is transferred from the protonated Schiff base to $Asp85^{BR}$, a counterion of the protonated Schiff base; at the same time, another proton is released from the proton-releasing group to the extracellular space (M-intermediate) (*14*). The Schiff base is then reprotonated by proton donor $Asp96^{BR}$ located on the cytoplasmic side (N-intermediate), followed by proton uptake from the cytoplasmic space. The retinal isomerizes back to the all-*trans* form, and $Asp96^{bR}$ is reprotonated (O-intermediate). Finally, a proton is transferred to the proton-releasing group from $Asp85^{bR}$, which returns BR to its original state. The crystal structures of unphotolyzed BR and various photointermediates have been obtained at high resolution (*15*−*18*). The essential mechanism of the type of proton transport carried out by BR has thus been established.

The photocycle of *Natronomonas (Natronobacterium) pharaonis* HR (NpHR) has intermediates analogous to BR (*19*, *20*). In the case of *H. salinarum* HR (HsHR), the O-intermediate does not accumulate, presumably for kinetic reasons (*21*). Mutagenesis studies of HsHR have revealed that $R108/T111^{HsHR}$ in the extracellular (EC) channel is a Cl^--binding site in the dark (*22*), which is consistent with an observation that $D85T^{BR}$ or $D85S^{BR}$ is converted into a light-driven Cl ion pump (*23*−*25*). It should be noted in this context that $R108^{HsHR}$ and $T111^{HsHR}$ correspond to $R82^{BR}$ and $D85^{BR}$, respectively.

† The work was in part supported by a Grant-in-Aid for JSPS Fellows from the Ministry of Education, Culture, Sports, Science and Technology, Japan.

* To whom correspondence should be addressed. Telephone and fax: +81-11-706-2771. E-mail: demura@sci.hokudaia.ac.jp.

‡ Graduate School of Science.

§ Graduate School of Pharmaceutical Sciences.

|| Center for Advanced Science and Technology.

[1] Abbreviations: BR, bacteriorhodopsin; CD, circular dichroism; CP, cytoplasmic; DM, *n*-dodecyl β-D-maltopyranoside; EC, extracellular; HR, halorhodopsin; HsHR, *H. salinarum* HR; NpHR, *N. pharaonis* HR.

10.1021/bi047500f CCC: $30.25
Published on Web 03/01/2005

The X-ray crystal structure of HsHR was determined at a resolution of 1.8 Å (*26*, *27*). The structure is most similar to that of BR (*28*) and *pharaonis* phoborhodopsin (*p*pR, also called "sensory rhodopsin II") (*29*, *30*), and the root-mean-square deviations (rmsds) on the main chain C_α atoms are 0.74 and 0.89 Å for BR and *p*pR, respectively, when the calculations are confined to the pentahelical C-G bundle. The crystal structure revealed that Cl^- is still hydrated by a cluster of three water molecules that form hydrogen bonds with the five neighboring amino acid residues, including $R108^{HsHR}$. The anion itself interacts with the proton of the protonated Schiff base and the hydroxyl group of $S115^{HsHR}$. It is of note that anion binding is observed in the crystal only at this position of the EC channel, implying that this Cl^- is transported to the cytoplasmic space by the photon.

It is assumed that a Cl^--binding or -interacting site in the cytoplasmic (CP) channel is required for the release of Cl^- to the cytoplasmic space, and this candidate has been suggested to be the Arg200/$Thr203^{HsHR}$ pair in CP (*22*). After release, the uptake of Cl^- through the EC occurs at the stage of O-decay, resulting in transport of Cl^- from the outside to the inside of the cells. With regard to uptake, $His95^{HsHR}$ has been suggested to be an important residue (*31*).

Although many HRs have been identified and reported (*2*, *32*−*34*), the investigations carried out to date have been conducted primarily using HsHR (*35*, *36*) and NpHR (*19*, *20*, *35*, *36*). Here, we used NpHR, which offered several advantages: (i) NpHR is more stable than HsHR; (ii) the retinal isomeric composition does not change with the light or dark adaptation conditions (*36*); (iii) NpHR transports not only halide ions but also nitrate at approximately the same rate (*37*); and (iv) a system of expression of archaeal rhodopsins has been reported using *Escherichia coli* as a host cell, which has been shown to be successfully applied to the preparation of large amounts of NpHR (*38*−*40*).

In this paper, we focused on addressing the following two issues using a mutation approach. The first issue was to clarify the Cl^--binding site in the unphotolyzed (ground) state of NpHR. Amino acid residues relevant to the bound site (i.e., $Arg123^{NpHR}$, $Thr126^{NpHR}$, and $Ser130^{NpHR}$) were chosen (see Figure 1) according to the X-ray crystal structure of HsHR and the results of a previous study (*22*). Here, $Arg123^{NpHR}$, $Thr126^{NpHR}$, and $Ser130^{NpHR}$ correspond to $Arg108^{HsHR}$, $Thr111^{HsHR}$, and $Ser115^{HsHR}$, respectively. $Arg108^{HsHR}$ interacts with Cl^-, forming a hydrogen bond through one water molecule (*26*). The reasons for focusing on this arginine residue are as follows: (i) it is positively charged, and (ii) it is a superconserved residue among archaeal rhodopsins. The second issue to be addressed was the identification of the putative Cl^--interacting (binding) site in the CP channel, whereby the candidate is thought to be $Lys215/Thr218^{NpHR}$ (corresponding to $Arg200/Thr203^{HsHR}$; see Figure 1). Spectrum changes in circular dichroism (CD) studies and investigation of the visible absorption induced by the addition of anions, as well as flash-photolysis experiments, revealed that these putative binding (or interacting) sites were indeed correct. On the basis of these observations, the putative HR Cl^- transport mechanism is considered in the Discussion.

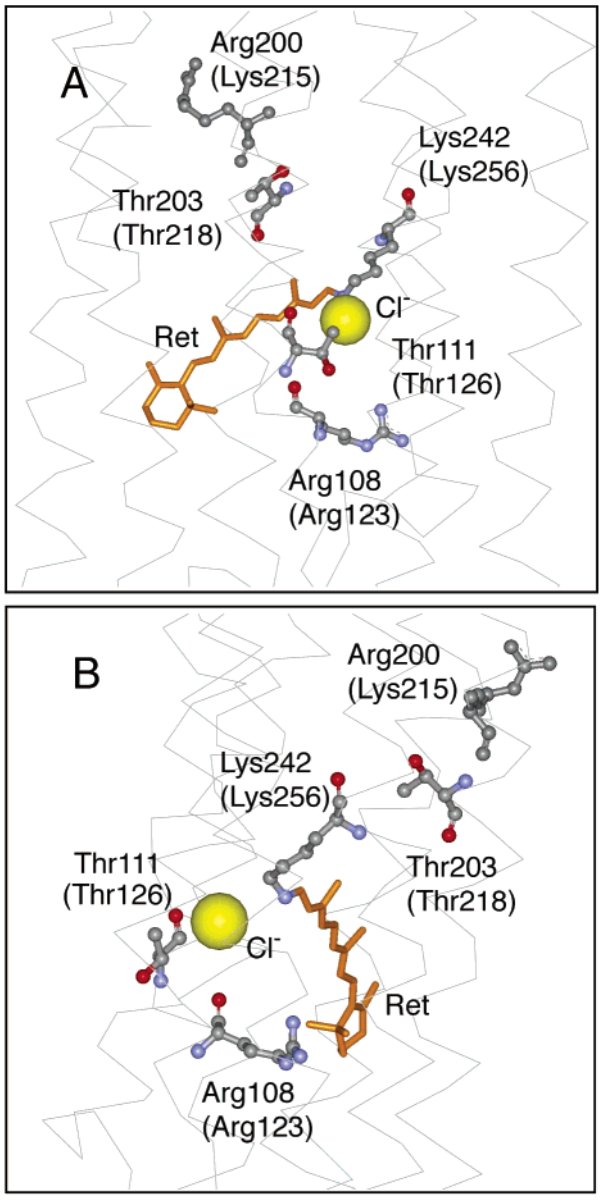

FIGURE 1: Putative Cl^--binding (interacting) site adapted from the X-ray structure of HsHR (halorhodopsin from *H. salinarum*) (PDB entry 1E12) (*26*). (A) Side view and (B) alternate side view of HsHR rotated ~90° about the vertical axis in panel A. The residues shown in parentheses correspond to residues in NpHR (HR from *N. pharaonis*, examined here). The region extending above the retinal is the cytoplasmic side, and in the opposite direction, the extracellular side is shown.

MATERIALS AND METHODS

Construction of Expression Plasmids of Mutants Bearing a Histidine Tag. Mutant plasmids for the expression of $Arg123^{NpHR}$, $Thr126^{NpHR}$, $Arg215^{NpHR}$, and $Thr218^{NpHR}$ mutants were constructed with a Quikchange site-directed mutagenesis kit (Stratagene Cloning Systems) and the modified pET-21c(+) vector to utilize the histidine-tagged region. The sequences of the primers designated to replace the Arg123, Thr126, Lys215, and Thr218 codon with other amino acid codons were 5′-ACG ATG TGG GGC AAA (for Lys)/CAC (for His) TAT CTG ACG TGG-3′ and 5′-CCA CGT CAG ATA TTT (for Lys)/GTG (for His) GCC CCA CAT CGT-3′ for the R123 mutant, 5′-GGC CGC TAT CTG GTG (for Val) TGG GCC CTT TCG-3′ and 5′-CGA AAG

GGC CCA CAC (for Val) CAG ATA GCG GCC-3′ for the T126V mutant, 5′-ATG TTC AAT ACG CTG AGG (for Arg)/CAG (for His) CTG CTG ACC GTT GT-3′ and 5′-AC AAC GGT CAG CCT (for Arg)/CTG (for His) CAG CGT ATT GAA CAT-3′ for the K215 mutant, and 5′-ACG CTG AAG CTG CTG GTC (for Val) GTT GTC ATG TGG CTC-3′ and 5′-GAG CCA CAT GAC AAC GAC (for Val) CAG CAG CTT CAG CGT-3′ for the T218V mutant. The mutations introduced into the plasmid were confirmed by DNA sequencing using a DNA sequencing kit (Applied Biosystems, Foster City, CA), and each mutated plasmid was introduced into BL21(DE3) cells. Transformed cells were selected by ampicillin resistance.

Protein Expression and Purification of NpHR. The protein expression and purification procedures using *E. coli* BL21-(DE3) cells harboring the plasmid have been described in detail in a previous paper (*40*). Fractions of the proteins using Ni−NTA agarose (Qiagen, Hilden, Germany) were collected by elution (flow rate, 56 mL/h) with buffer E {50 mM Tris-HCl (pH 7.0), 300 mM NaCl, 150 mM imidazole, and 0.1% *n*-dodecyl β-D-maltopyranoside [dodecyl maltoside (DM)] (Dojindo Lab, Kumamoto, Japan)}. The yields of the wild-type and mutant NpHRs were almost the same, as was that of T126V, as reported previously (*41*).

Preparation of the Blue Species. The anion-free blue species of wild-type NpHR and the mutants were prepared by interchanging the buffer with buffer C [10 mM 2-morpholinopropanesulfonic acid, MOPS (pH 7.0), and 0.1% DM] by passing the species over a Sephadex-G25 column (2.5 cm × 20 cm, Amersham Pharmacia Biotech, Uppsala, Sweden) at a flow rate of 2 mL/min. After the buffer exchange, the protein concentration of the mutants was estimated using an extinction coefficient (ϵ_{600}) of 50 000 M^{-1} cm^{-1} for wild-type NpHR (*42*).

CD and Absorption Measurements. The CD spectra of both wild-type and mutant NpHRs were measured with a Jasco J-725 spectropolarimeter (Jasco, Tokyo, Japan) in the 300−750 nm region at 25 °C at a scanning speed of 200 nm/min, and accumulation was carried out twice. The measuring medium was buffer C containing various concentrations of NaCl (0.1, 0.2, 0.5, 1, 2, 3, 4, 5, 10, 20, 30, 50, 100, 150, 200, 400, 600, and 1000 mM). The protein concentration was 18 μM. The path length of the optical cuvette was 10 mm. The absorption spectra were measured with a UV mini 1240 spectrometer (Shimadzu, Kyoto, Japan).

Flash Photolysis Spectroscopy. A computer-controlled flash-photolysis apparatus was constructed as described in a previous paper (*43*). An actinic light source (λ = 532 nm, 7 ns, ∼5 mJ pulse) was the second harmonic of the fundamental beam of a Q-switched Nd:YAG laser (Surelite I-10; Continuum). This actinic laser flash was polarized vertically with a Glan laser polarizer (PLU-10; Optics for Research) placed just in front of the sample cells (10 mm × 10 mm quartz cuvette), and the interval of the measurements was 1 s. The absorbance of the sample in 1 M NaCl [containing 10 mM MOPS (pH 7.0) and 0.1% DM] was 0.5 at the absorption maximum, and the temperature was maintained at 20 °C. The source of the monitoring light was a 150 W xenon arc lamp (C4251; Hamamatsu Photonics, Hamamatsu, Japan), and the beam of the monitoring light was perpendicular to that of the actinic flash. In the case of the measurement at 660−750 nm, a Y43 filter (Toshiba, Tokyo, Japan) was used to cut the UV light. A photomultiplier (R2949; Hamamatsu Photonics) was used to detect the monitoring light passing through the sample. To select the measuring wavelength and exclude the scattered actinic flash from the sample, two monochromators were placed behind the monitoring light source and in front of the photomultiplier. The output of the photomultiplier was amplified by a homemade $I-V$ converter with an offset voltage. In a computer equipped with an A/D converter, the amplified data were stored and averaged. The observed data were recorded between −26 and 136 ms every 0.8 μs for WT and T126V, and between −44 and 218 ms every 0.5 μs for other mutants. The original data were collected 50−100 times for each sample. Then, data points on a logarithmic time scale were picked up from the observed data for the following data analysis.

Data Analysis of Photocycling. We adopted two methods to determine the lowest number of exponential terms required to fit the observed kinetic data. One of these methods employed SVD analysis with Igor software (WaveMetrics, Inc.). Independently, the data observed at all wavelengths from 410 to 710 nm were fitted simultaneously with the following multiexponential equation:

$$\Delta A(\lambda,t) = \sum_{i=1}^{n} B_i(\lambda) \exp(-t/\tau_i) \tag{1}$$

Considering the results of these two methods, n was determined. Here, τ_i of eq 1 represents the decay time constant of the ith component that is expressed as P_i, the photochemically defined intermediate, according to Chizhov and Engelhard (*20*).

$$P_0(\text{NpHR}) \rightarrow P_1 \xrightarrow{\tau_1} P_2 \xrightarrow[\cdots]{\tau_2} P_i \xrightarrow{\tau_i} P_o(\text{NpHR})$$

The P_i is permitted to be a mixture of physically defined photointermediates. The $B_i(\lambda)$ term in eq 1 is formulated as

$$B_i(\lambda) = F_c \sum_{j=i}^{n} a_{i,j} \Delta\epsilon_j(\lambda) \; (i = 1 - n) \tag{2}$$

where

$$a_{i,j} = \frac{1}{\prod_{m=1}^{j-1} \tau_m \prod_{\substack{m=1 \\ m \neq i}}^{j} (1/\tau_m - 1/\tau_i)}$$

and $\Delta\epsilon_j(\lambda)$ stands for the absorption difference between P_i and P_0(NpHR) at wavelength λ when all P_0(NpHR) molecules in the cuvette are photolyzed. F_c is the fraction of the P_0 molecule that is activated by the flash to undergo the photocycle. Equation 2 indicates that the B spectra of the nth, i.e., the last, component is given by

$$B_n(\lambda) = F_c a_{nn} \Delta\epsilon_n(\lambda)$$

$$a_{nn} = \frac{1}{\prod_{m=1}^{n-1} (1 - \tau_m/\tau_n)} \tag{3}$$

meaning that $F_c\Delta\epsilon_n(\lambda)$ can be determined from $B_n(\lambda)$, which is already known from the fitting with eq 1. Once $F_c\Delta\epsilon_n(\lambda)$ of the nth component is determined, $F_c\Delta\epsilon_{n-1}(\lambda)$ of the $(n-1)$th component can be easily determined using eq *2*. Then, we can determine $F_c\Delta\epsilon_i(\lambda)$ for all components iteratively under an appropriate order of time constants (τ_1, τ_2, ..., τ_n) in the photocycle. The negative part of $F_c\Delta\epsilon_i(\lambda)$ should originate from only the depletion of P_0 by the flash excitation. The criterion for determining the order, thus, is the absence of a negative part except for the P_0 absorption band. Then, we examined all possible sequences of their order for the calculation of $F_c\Delta\epsilon_i(\lambda)$, and the best sequence was chosen. Finally, the addition of the F_c times spectrum of the original NpHR gives the spectrum of P_i. The value of F_c was determined so that the evaluated spectra, composed of mainly a single physically defined intermediate, would conform to the skewed Gaussian function (*44*).

RESULTS

Titration of the Wild-Type and Mutant NpHRs with Chloride on Visible CD and Absorption Spectra. The Cl^--free form (blue species) of the wild type and the mutant NpHRs were titrated with NaCl to obtain the CD spectra in the visible region (450−700 nm). Figure 2 shows the spectra obtained in the presence of 0 and 1 M NaCl. As shown in this figure, a bilobe in the visible region is shown. This result is a good agreement with CD spectra of NpHR purified from *N. pharaonis* (*42*) and a previous report (*45*). A similar relationship between the exciton band and the oligometic states of BR has been reported (*46*−*48*), suggesting that NpHR also forms an oligomer. In this study, therefore, by gel filtration on agarose columns and dynamic light scattering, the apparent molecular mass of the wild-type NpHR used in this study was determined to be 340−430 kDa, indicating the association composed of 8−11 monomers even in the DM detergent (data not shown). Therefore, Figure 2 indicates that all mutants, and wild-type NpHR, exist not as monomers but associated at all salt concentrations (*20*, *41*, *49*).

The magnitude of the negative component of the exciton band of R123K (Figure 2B) was smaller than that of the positive component. The reason for this result is not known, but it is possible that replacement of $Arg123^{NpHR}$ with Lys may have altered the structure around the retinal. The addition of NaCl, except in the case of R123H (Figure 2C), changed the CD band in two ways: (i) the crossover points were blue-shifted, and (ii) the magnitude of the positive component of the exciton band increased with the negative component being held steady (this trend remained basically constant among samples). For the K215R, K215Q, and T218V mutants, the spectrum changes were almost the same as those of wild-type NpHR.

The interaction with NaCl was also examined from another perspective. Figure 3 shows the visible spectrum changes obtained by titration with NaCl. With the exception of R123K and R123H, the addition of NaCl shifted the maximum wavelength to a shorter wavelength, with increases in the extinction coefficient; these findings are consistent with the blue shift of the crossover point of the CD spectra. R123K was found to have the opposite tendency compared to the other NpHRs with respect to the maximum wavelength shift

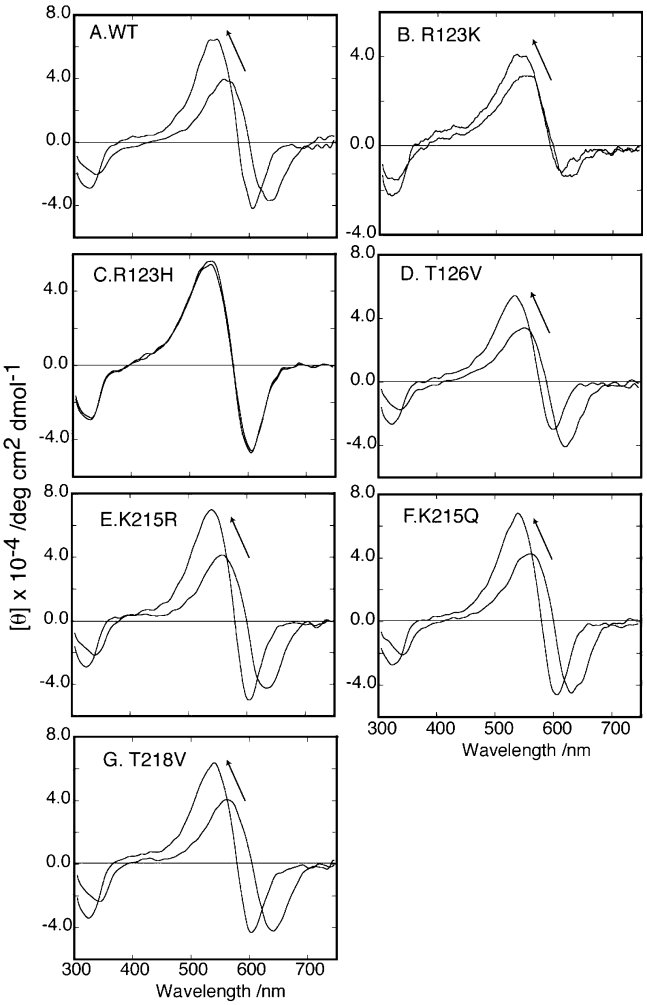

FIGURE 2: Chloride-dependent changes in the circular dichroic spectra of wild-type NpHR (A) and mutants [(B) R123K, (C) R123H, (D) T126V, (E) K215R, (F) K215Q, and (G) T218V]. For measurements carried out under Cl^--free conditions, spectra were obtained in 10 mM MOPS (pH 7.0) and 0.1% DM. The protein concentration was 18 μM. For the measurements of the Cl^--bound form, 1 M NaCl was used. The volume changes due to the addition of the concentrated NaCl solution were corrected. The measurements were carried out at 25 °C. The arrows indicate the spectral shift resulting from the addition of Cl^-.

(except for R123H), although the magnitude of the shift was very small. This result might have been related to the asymmetric CD spectrum of the exciton coupling; indeed, it was noted that for HsHR, the addition of halogen anions to the blue HsHR induced a red shift of the absorption maximum (*48*), as was the case with the R123K mutant.

The observed shifts in the wavelength of the absorption maximum ($\Delta\lambda$) were analyzed using the following adsorption isotherm equation:

$$\Delta\lambda = \Delta\lambda_{max}\frac{[\text{anion}]}{K_d + [\text{anion}]}$$

where $\Delta\lambda_{max}$ and K_d represent the maximum shift of the wavelength and the dissociation constant, respectively. The estimated K_d values are shown in Table 1. When the Hill coefficient (*40*) was introduced, this value for the wild type and mutants was estimated to be unity and no changes in K_d were observed.

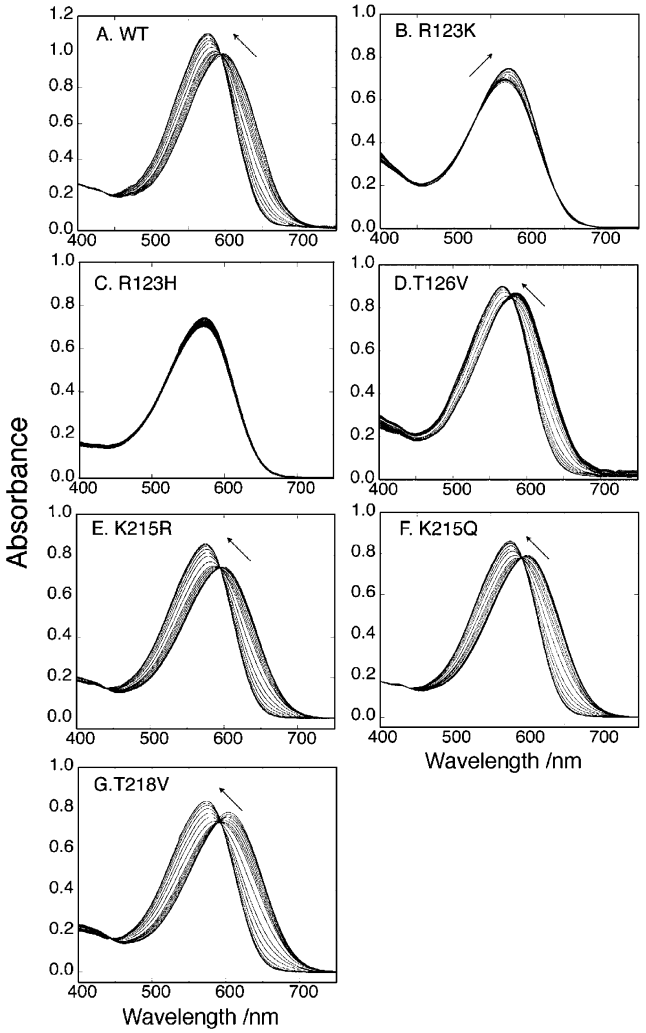

FIGURE 3: Chloride-dependent changes in the absorption spectrum of wild-type NpHR (A) and mutants [(B) R123K, (C) R123H, (D) T126V, (E) K215R, (F) K215Q, and (G) T218V]. The arrows indicate a spectral shift resulting from the addition of NaCl. Concentrations of NaCl were 0, 0.1, 0.2, 0.5, 1, 2, 3, 4, 5, 10, 20, 30, 50, 100, 150, 200, 400, 600, and 1000 mM. The experimental conditions were the same as those described in the legend of Figure 2.

Table 1: Shifts of Absorption Maxima (λ_{max}) upon Addition of Various Salts to Anion-Free NpHR Samples, and K_d Values for Cl^- Binding[a]

	λ_{max} (nm)				
	none	NaBr	NaCl	$NaNO_3$	K_d for Cl^- (mM)
wild type	600	576	577	562	5
R123K	569	571	575	570	39
R123H	571	572	573	572	−
T126V[b]	584	565	567	554	32
K215R	599	576	574	569	5
K215Q	600	578	576	571	4
T218V	603	577	573	566	7

[a] The values of λ_{max} of the anion-bound form were obtained in the presence of 1 M salt (pH 7.0 and 25 °C). The determination of the dissociation constants is described in the text. [b] Data from ref *41*.

In the case of the R123H mutant (note that $Arg123^{NpHR}$ was located in the EC channel), an insensitive visible absorption shift after addition of Cl^- was observed compared with other mutants, although the oligomeric structure was not changed as shown in the exciton band of the CD spectra, suggesting that the R123H mutation changes only local structure corresponding to the Cl^--binding site of the chromophore (*26*). On the other hand, when Lys215 or Thr218, the putative Cl^--interacting residues in the CP channel, was mutated, essentially no changes in binding affinity were observed. These findings revealed that in the unphotolyzed state, Cl^- binds to the site composed of $Arg123^{NpHR}$ and $Thr126^{NpHR}$ in the EC channel, and not to the putative site composed of $Lys215^{NpHR}$ and $Thr218^{NpHR}$ in the CP channel.

Flash-Induced Absorbance Changes in Wild-Type and Mutant NpHRs. As described in Materials and Methods, flash-photolysis experiments were performed in 1 M NaCl; in those experiments, the wild type and all of the mutant NpHRs were considered to be in the Cl^--bound form, because the K_d values were 5 mM for the wild type and 5−40 mM for all of the mutants. Because the $R123H^{NpHR}$ mutant indicated no visible spectral shift after titration of Cl^-, no flash-photolysis experiments were carried out. The scattered laser flash caused a strong artifact at the beginning of the trace, and therefore, the optical data were reliably evaluated after 10 μs. The flash-induced difference spectra for wild-type and mutant NpHRs are shown in Figure 4, indicating the presence of two positive bands (490 and 640 nm) and a negative band at 580 nm, due to the depletion of the original NpHR. The positive bands at 490 and 640 nm are assigned to the L- and O-intermediates, respectively. Since the decay lifetime of the K-intermediate is 0.4 μs (*20*), we could not observe this intermediate.

Figure 4 reveals the following features characteristic of and common to two types of mutants. One type of mutant was termed the "EC mutant", in which an amino acid residue constituting the putative Cl^--binding site in the EC region ($Arg123^{NpHR}$ and $Thr126^{NpHR}$) was mutated. The other type of mutant was termed the "CP mutant", in which a putative anion-interacting site in the CP region, $Lys215^{NpHR}$ or $Thr218^{NpHR}$, was mutated. The EC mutant had two photointermediates (L and O), which was also the case in wild-type NpHR, but the rate of photocycling, especially the rate at the last step, was slower than that of the wild-type protein. On the other hand, the CP mutant lacked the O-intermediates, and the cycling rate appeared to be prolonged, except in the case of K215Q.

The data observed at all wavelengths from 410 to 710 nm were fitted simultaneously with multiexponential eq 1 as described in Materials and Methods, and the number of exponential terms was three for the wild type, R123K, T126V, and K215Q and two for K215R and T218V. The flash-photolysis data were analyzed as described above. Figure 5 shows the results of the data analysis. The leftmost column shows the *B* spectra, and the spectra of P_i are shown in the order of their appearance after the flash. For wild-type NpHR, the spectra of P_1 and P_2 were almost the same, and the absorption maximum was ca. 520 nm in both cases. Therefore, the main components of these two intermediates are identified as L1 and L2. The spectrum of P_3 had two absorption maxima, indicating that P_3 is composed of two physically defined intermediates that attain equilibrium at a rate much faster than the rate of decay. The spectrum was separated with the aid of skewed Gaussian fitting (*44*), and the results are shown in the right portion of Figure 5. This separation indicates a mixture of L- and

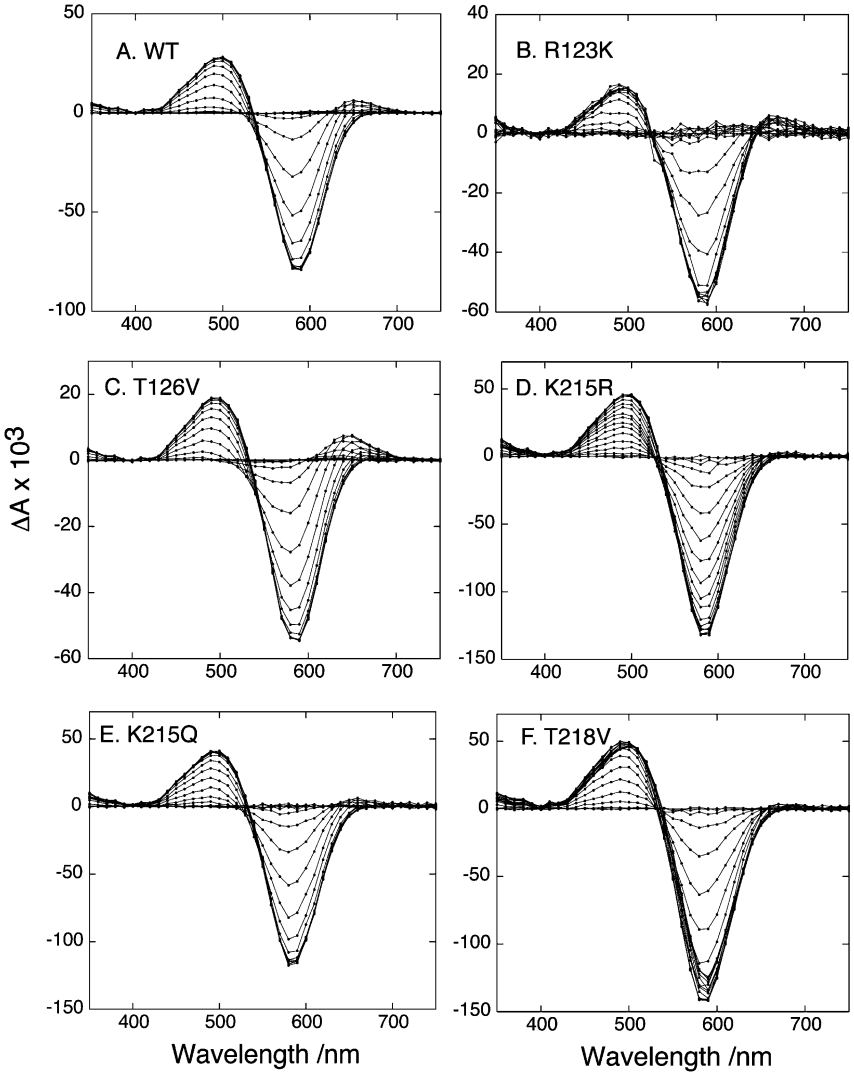

FIGURE 4: Flash-induced light minus dark difference spectra of the Cl^--bound form of wild-type NpHR (A) and various mutants of NpHR [(B) R123K, (C) T126V, (D) K215R, (E) K215Q, and (F) T218V]. The first spectrum showing the most substantial depletion at 580 nm was that obtained 10 μs after the flash. Because of the large scattering effects of the laser flash, this range of time was the shortest to be measured. The last duration for the acquisition was 103 ms for wild-type NpHR and the T126V mutant, and 122 ms for the other mutants. The experimental conditions were the same as those described in the legend of Figure 2. Because R123H does not bind with Cl^-, no experiments were carried out using this mutant. The data (●) were acquired every 10 nm, and the spectra picked up in a logarithmic time scale from 10 μs to 120 ms are shown.

O-intermediates, with a larger contribution from the O-intermediate. In the case of R123K, although the spectra of P_1 and P_2 appeared to include a minor component showing absorption of a longer wavelength, these components were identified as L1 and L2. P_3 of this mutant was not the O-intermediate, because the absorption maximum was almost the same as that of P_0(NpHR). Therefore, we recognized this intermediate as NpHR′ [or as N, according to Chizhov and Engelhard (*20*)]. The spectrum of P_3 of the T126V mutant appeared to contain a small amount of a component showing absorption at the longer wavelength, but we identified this component as NpHR′(N), i.e., as the main component. For K215R and T218V, simulation using two exponential terms was sufficient to fit the data, and both intermediates (P_1 and P_2) were recognized as L1 and L2, respectively, thus indicating a lack of the O-intermediate, as shown in Figure 4. On the other hand, P_3 of K215Q was found to have a ternary complex of O, L2, and NpHR′(N). In Figure 6, the summarized scheme of sequences of intermediates is shown together with the decay time constant (in microseconds) of each intermediate. In the L1 → L2 transition, the time constant of the wild type was slightly different from that of Chizhov and Engelhard (*20*). This may come from the difference in experimental conditions such as sample preparation using the recombinant system and pH.

DISCUSSION

We examined the binding of Cl^- and other anions to blue anion-free NpHR by CD and analysis of the visible absorption spectra (Figures 2 and 3 and Table 1). The CP mutants exhibited changes similar to those of the wild type. On the other hand, the EC mutants (especially the Arg123 mutant) exhibited spectrum changes that differed from those of the wild type: R123H exhibited no binding and R123K weak binding. In the case of R123K, the positively charged lysine residue might have played a role in the red shift of the absorption maximum upon addition of Cl^- to anion-free NpHR instead of the positively charged arginine residue. It was noted that the pattern of binding estimated from the shift in the absorption maximum (Figure 3) agreed well with that

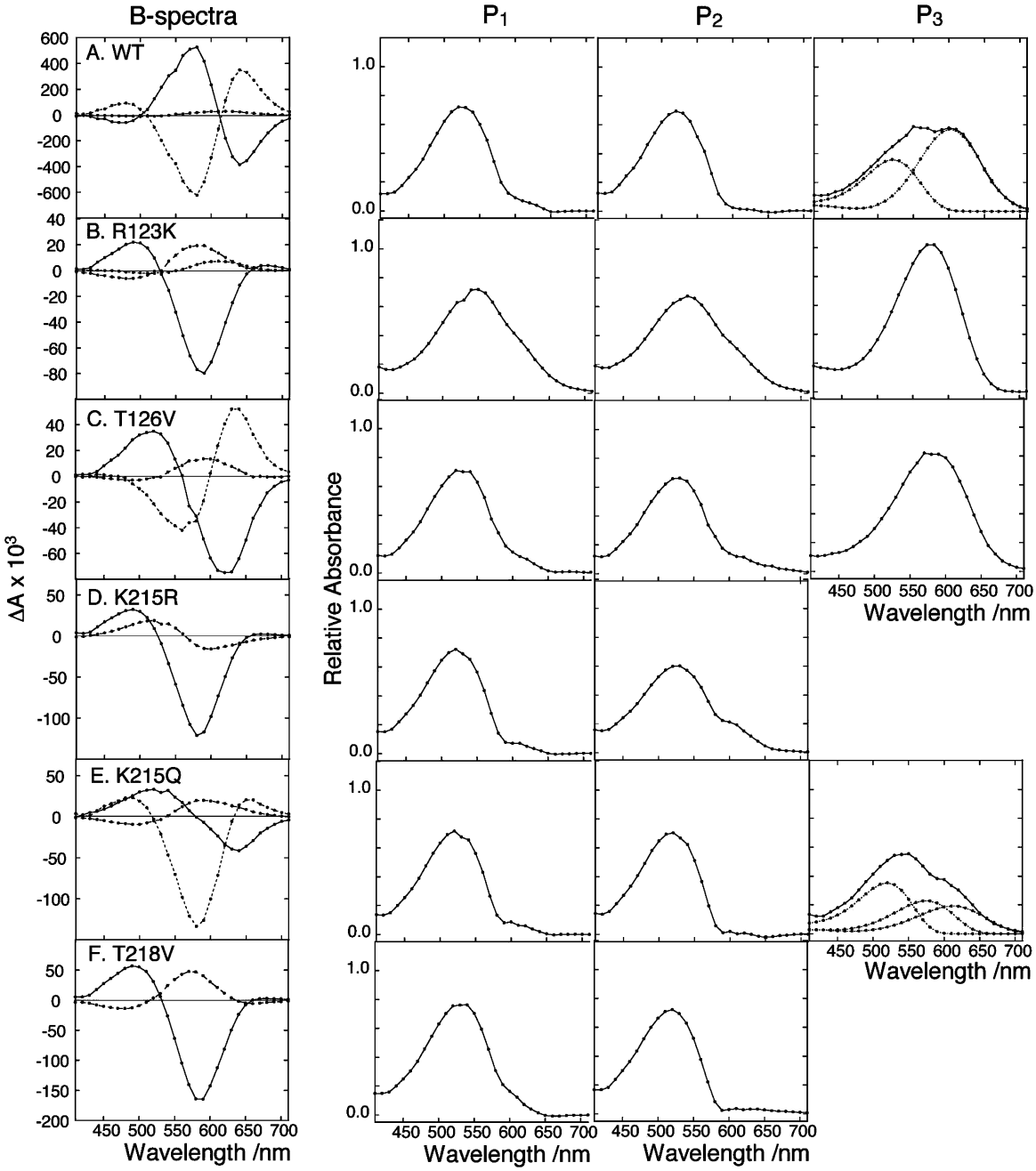

FIGURE 5: Results of the global fitting of the flash-photolysis data of wild-type NpHR (A) and mutants [(B) R123K, (C) T126V, (D) K215R, (E) K215Q, and (F) T218V]. The data (●) were taken from those shown in Figure 4. The column at the far left represents the *B* spectra (explanation given in the text). The second column from the left shows the spectra of P_1, which was the first spectroscopically identified photointermediate after the flash. The spectra of P_2 are shown in the third column. The right-most column shows the spectra of P_3, which was the third spectroscopically identified photointermediate. Some of the spectra are composed of two physically identified photointermediates. The dotted lines show the spectra of the components (physically defined intermediates), shown separately from the P_3 spectra using the skewed Gaussian function described in the text.

of the binding isotherm with only one binding site. This suggests that there is only one binding site near the Schiff base in the EC region. Since the observed color change might have been influenced only by the changes near the chromophore, we cannot rule out the possibility of another binding site far from the chromophore. However, the crystal structure of HsHR revealed only one Cl^--binding site (*26*). We therefore concluded that there is one anion-binding site in the EC region near the Schiff base in the unphotolyzed state of NpHR, which was the same as that of HsHR. This anion is thought to be transported by a photon to the cytoplasmic space through the CP channel.

Previously, we examined the contribution of $Ser130^{NpHR}$ ($Ser115^{HsHR}$) to Cl^- binding, and mutation at this position (S130A, S130C, and S130T) was found to increase the dissociation coefficient to 89−159 mM Cl^- (*49*). Taken together, the previous results and the results presented here suggest that anion binding preferentially takes place in the following order: $Arg123^{NpHR}$ > $Ser130^{NpHR}$ > $Thr126^{NpHR}$. This finding is partially consistent with a previous observation that the hydroxyl group of $Thr111^{HsHR}$ ($Thr126^{NpHR}$) was shown to be superfluous for Cl^- binding in the case of HsHR (*22*). Note that the X-ray crystal structure of HsHR revealed that the hydroxyl group of $Thr111^{HsHR}$ (corresponding to

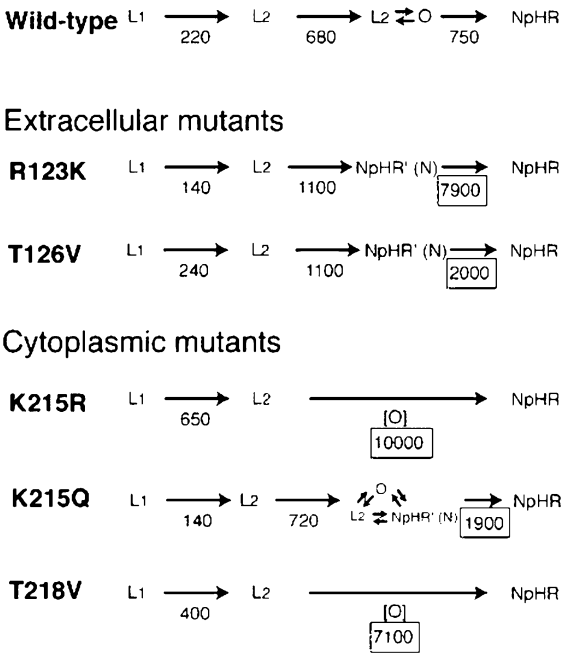

FIGURE 6: Summary of the photocycling scheme of wild-type NpHR and the mutants. The numbers indicate the time constants of the respective transitions, measured in microseconds. The numbers enclosed in boxes show the time constants that differed largely from those of wild-type NpHR.

Thr126^{NpHR}) interacts with palmitate, and not with the bound Cl^- (*26*). However, our results indicated that Thr126^{NpHR} does play a role in binding in the case of NpHR.

The flash-photolysis data are summarized in Figure 6. The characteristic features of the EC mutants (R123K and T126V) were as follows: (1) the time constants of the transition from L1 to L2 and the rate of decay of L2 did not essentially differ from those of wild-type NpHR, and (2) the greatest difference from the wild-type protein was the significant slow transition in the last intermediate of the photocycle, which was assigned to NpHR′(N). On the other hand, it was of note that the photocycle of the CP mutants (except for K215Q) lacked the O-intermediate. This probably means that the O-intermediate was not accumulated kinetically because the rate of L2 decay was very slow.

On the basis of the observations reported here, the following hypothetical mechanism of Cl^- transport by HR appears to be reasonable. Essen (*27*) also presented his scheme on the transport mechanism. At the unphotolyzed state, Cl^- binds to the EC binding site due to interaction with a Schiff base, Arg123^{NpHR} (Arg108^{HsHR}), Thr126^{NpHR} (Thr111^{HsHR}), and Ser130^{NpHR} (Ser115^{HsHR}). The greatest contribution to binding among these residues was found to be made by the arginine residue. In fact, the crystal structure of HsHR revealed that the C═O and NH_2 groups of this arginine residue form hydrogen bonds with Cl^- through one water molecule for each hydrogen bond (*26*).

Illumination induces the retinal conformational change from all-*trans* to 13-*cis* 15-*anti*, which results in the distortion around the surroundings of the retinal Schiff base close to the Cl-binding site and the change in the orientation of its NH dipole. As already shown in the case of BR (*50*), the orientation of the guanidinium of Arg123^{NpHR} might change, or a conformational change around the arginine residue might take place, although no direct evidence has been reported

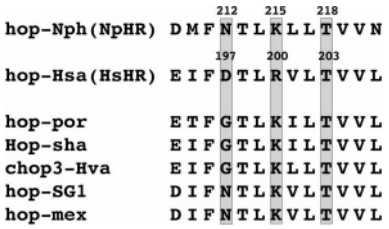

FIGURE 7: Alignment of the amino acid residues of NpHR and HsHR around the putative Cl^--binding (interacting) site in the CP region. These residues are located in the F-helix and are occluded from access to the cytosol in the dark. Protein comparisons were carried by using the Pileup program in the University of Wisconsin Genetics Computer Groups (GCG) package. The references to halorhodopsin and the sources, from the top, are as follows: hop-Nph, *N. pharaonis* HR (GenBank entry J05199); hop-Hsa, *H. salinarum* HR (GenBank entry X04777); hop-por, port hR (GenBank entry D43766); hop-sha, shark hR (GenBank entry D43765); chop3-Hva, cruxhalorhodopsin-3 (GenBank entry D31881); hop-SG1, SG1 hR (GenBank entry X70292); and hop-mex, mex hR (GenBank entry D11136).

for HR. These two changes weaken Cl^- binding, and Cl^- is translocated from the EC binding site to the Cl^--interacting site in the CP region; this site is formed by Lys215^{NpHR} (Arg200^{HsHR}) and Thr218^{NpHR} (Thr203^{HsHR}) located in helix F. Mutation at these positions causes a loss of the interacting (or binding) site, and induces the significantly slow decay of L2, which in turn gives rise to the lack of the O-intermediate due to the kinetics. The observation that a mutation in the CP region modulated the decay of the L2-intermediate suggests that during the decay of the L2-intermediate, Cl^- is translocated into the CP channel. K215Q bears the complex component of P_3, and in this mutant, the presence of the O-intermediate was detected. This finding indicated that the O-intermediate was present in small amounts in this mutant, although it is unknown whether the K215Q pumps Cl^-. On the other hand, the T218V mutant completely lacked the O-intermediate. This result suggests that the threonine residue (Thr218^{NpHR}) makes a more significant contribution to the interaction of Cl^-. Note that this threonine residue was conserved for all HRs (see Figure 7). In a light-driven Cl^--transporting D85T mutant of BR, the arginine residue (corresponding to Lys215^{NpHR}) was not found to be important (*24*).

If the cytoplasmic opening or outward tilting of helix F occurs during the L2 → O transition phase, as in BR and *pp*R (NpsRII) (*50*−*55*), hydrophilicity may increase along the cytoplasmic region of helix F, and water may enter along the helix. This might in turn give rise to the hydration of Cl^- in the CP interaction site, which induces the dissociation of Cl^- from the threonine residue, and then, the Cl^- is released into the cytoplasmic space. We could not rule out the possibility of an additional force leading to the release of Cl^- from the interacting site, which would push the anion outside of the protein. Hackmann et al. (*56*) observed large changes in the amide I bands of a Fourier transform infrared spectrum during the L2 → O transition, and these changes were indicative of large conformational changes in HR, thus providing support for opening of the F-helix. The mutant lacking this interacting site was unable to efficiently release Cl^-. The interaction between Cl^- and the NH dipole of the Schiff base might hinder the conformational change of the retinal from 13-*cis* to all-*trans*, which is the basic process of O-intermediate formation, because the NH dipole is

oriented toward the extracellular side in the all-*trans* conformation. In other words, the release of Cl^- might be indispensable for formation of the O-intermediate. For this reason, the CP mutants showed a slow decay of L2.

After the release of Cl^- to the cytoplasmic space, the F-helix might return to its original position. During the decay of the O-intermediate, Cl^- enters the protein toward the original binding site through the EC channel. Previously, we suggested the hypothesis that this process is passive, based on stopped-flow experiments (*40*). In this context, it becomes relevant to consider why R123K and T126V have an intermediate of NpHR′ (or an N-intermediate). If the conformational change around $Arg123^{NpHR}$ takes place (which may be one factor leading to the translocation of Cl^- from the EC to the CP space, as described above), then restoration to the original conformation should occur. It then becomes reasonable to suggest that the transition from HR′ to HR could be associated with the restoration of some residues around $Arg123^{NpHR}$ or its own orientation, as assumed by Essen (*27*). This prompt restoration may require the cooperation of the threonine residue, or of other residues around the EC binding site.

The K215R mutant of NpHR has the same residue pair at the interacting site in the CP channel as wild-type HsHR (see Figure 7). Surprisingly, the introduction of arginine at this position was found to substantially retard the L2 decay. The X-ray crystal structure of HsHR revealed an interaction between $Arg200^{HsHR}$ and $Asp197^{HsHR}$, which might reduce the positive charge of the guanidinium (*26*). The residue in NpHR that corresponds to this $Asp197^{HsHR}$ is $Asn212^{NpHR}$, whereas in the case of the K215R mutant, the positive charge of the introduced Arg cannot be offset. This suggests that the presence of a positive charge at this position is not favorable for efficient Cl^- pumping. To investigate this possibility, a $K215R/N212D^{NpHR}$ double mutant would be necessary, but unfortunately, this mutant was not expressed. The question of why lysine is located at this position of all HRs, except for in the case of HsHR (see Figure 7), despite its disadvantageous positive charge remains to be answered. Future studies will still be needed to clarify the role played by this residue. In addition, the putative Cl^- transport mechanism described above requires further confirmation.

REFERENCES

1. Matsuno-Yagi, A., and Mukohata, Y. (1980) ATP synthesis linked to light-dependent proton uptake in a rad mutant strain of *Halobacterium* lacking bacteriorhodopsin, *Arch. Biochem. Biophys. 199*, 297−303.
2. Mukohata, Y., Ihara, K., Tamura, T., and Sugiyama, Y. (1999) Halobacterial rhodopsins, *J. Biochem. 125*, 649−657.
3. Oesterhelt, D. (1995) Structure and function of halorhodopsin, *Isr. J. Chem. 35*, 475−494.
4. Schobert, B., and Lanyi, J. K. (1982) Halorhodopsin is a light-driven chloride pump, *J. Biol. Chem. 257*, 10306−10313.
5. Váró, G. (2000) Analogies between halorhodopsin and bacteriorhodopsin, *Biochim. Biophys. Acta 1460*, 220−229.
6. Oesterhelt, D., and Stoeckenius, W. (1971) Rhodopsin-like protein from the purple membrane of *Halobacterium halobium*, *Nat. New Biol. 233*, 149−152.
7. Lanyi, J. K. (2004) Bacteriorhodopsin, *Annu. Rev. Physiol. 66*, 665−688.
8. Haupts, U., Tittor, J., and Oesterhelt, D. (1999) Closing in on bacteriorhodopsin: Progress in understanding the molecule, *Annu. Rev. Biophys. Biomol. Struct. 28*, 367−399.
9. Booth, P. J., Templer, R. H., Curran, A. R., and Allen, S. J. (2001) Can we identify the forces that drive the folding of integral membrane proteins? *Biochem. Soc. Trans. 29*, 408−413.
10. Oesterhelt, D., Tittor, J., and Bamberg, E. (1992) A unifying concept for ion translocation by retinal proteins, *J. Bioenerg. Biomembr. 24*, 181−191.
11. Oesterhelt, D. (1998) The structure and mechanism of the family of retinal proteins from halophilic archaea, *Curr. Opin. Struct. Biol. 8*, 489−500.
12. Lanyi, J. K. (1997) Mechanism of ion transport across membranes. Bacteriorhodopsin as a prototype for proton pumps, *J. Biol. Chem. 272*, 31209.
13. Lozier, R. H., Bogomolni, R. A., and Stoeckenius, W. (1975) Bacteriorhodopsin: A light-driven proton pump in *Halobacterium halobium*, *Biophys. J. 15*, 955−962.
14. Balashov, S. P., Lu, M., Imasheva, E. S., Govindjee, R., Ebrey, T. G., Othersen, B., Chen, Y., Crouch, R. K., and Menick, D. R. (1999) The proton release group of bacteriorhodopsin controls the rate of the final step of its photocycle at low pH, *Biochemistry 38*, 2026−2039.
15. Luecke, H., Schobert, B., Richter, H. C., Cartailler, J. P., and Lanyi, J. K. Structure of bacteriorhodopsin at 1.55 Å resolution, *J. Mol. Biol. 291*, 899−911.
16. Takeda, K., Matsui, Y., Kamiya, N., Adachi, S., Okumura, H., and Kouyama, T. (2004) Crystal structure of the M intermediate of bacteriorhodopsin: Allosteric structural changes mediated by sliding movement of a transmembrane helix, *J. Mol. Biol. 341*, 1023−1037.
17. Neutze, R., Pebay-Peyroula, E., Edman, K., Royant, A., Navarro, J., and Landau, E. M. (2002) Bacteriorhodopsin: A high-resolution structural view of vectorial proton transport, *Biochim. Biophys. Acta 1565*, 144−167.
18. Schobert, B., Brown, L. S., and Lanyi, J. K. (2003) Crystallographic structures of the M and N intermediates of bacteriorhodopsin: Assembly of a hydrogen-bonded chain of water molecules between Asp-96 and the retinal Schiff base, *J. Mol. Biol. 330*, 553−570.
19. Váró, G., Needleman, R., and Lanyi, J. K. (1995) Light-driven chloride ion transport by halorhodopsin from *Natronobacterium pharaonis*. 2. Chloride release and uptake, protein conformation change, and thermodynamics, *Biochemistry 34*, 14500−14507.
20. Chizhov, I., and Engelhard, M. (2001) Temperature and halide dependence of the photocycle of halorhodopsin from *Natronobacterium pharaonis*, *Biophys. J. 81*, 1600−1612.
21. Váró, G., Zimányi, L., Fan, X., Sun, L., Needleman, R., and Lanyi, J. K. (1995) Photocycle of halorhodopsin from *Halobacterium salinarium*. *Biophys. J. 68*, 2062−2072.
22. Rüdiger, M., and Oesterhelt, D. (1997) Specific arginine and threonine residues control anion binding and transport in the light-driven chloride pump halorhodopsin, *EMBO J. 16*, 3813−3821.
23. Kalaidzidis, I. V., and Kaulen, A. D. (1997) Cl^--dependent photovoltage responses of bacteriorhodopsin: Comparison of the D85T and D85S mutants and wild-type acid purple form, *FEBS Lett. 418*, 239−242.
24. Paula, S., Tittor, J., and Oesterhelt, D. (2001) Roles of cytoplasmic arginine and threonine in chloride transport by the bacteriorhodopsin mutant D85T, *Biophys. J. 80*, 2386−2395.
25. Sasaki, J., Brown, L. S., Chon, Y. S., Kandori, H., Maeda, A., Needleman, R., and Lanyi, J. K. (1995) Conversion of bacteriorhodopsin into a chloride ion pump, *Science 269*, 73−75.
26. Kolbe, M., Besir, H., Essen, L. O., and Oesterhelt, D. (2000) Structure of the light-driven chloride pump halorhodopsin at 1.8 Å resolution, *Science 288*, 1390−1396.
27. Essen, L. O. (2002) Halorhodopsin: Light-driven ion pumping made simple? *Curr. Opin. Struct. Biol. 12*, 516−522.
28. Pebay-Peyroula, E., Rummel, G., Rosenbusch, J. P., and Landau, E. M. (1997) X-ray structure of bacteriorhodopsin at 2.5 Å from microcrystals grown in lipidic cubic phases, *Science 277*, 1676−1681.
29. Royant, A., Nollert, P., Edman, K., Neutze, R., Landau, E. M., Pebay-Peyroula, E., and Navarro, J. (2001) X-ray structure of sensory rhodopsin II at 2.1-Å resolution, *Proc. Natl. Acad. Sci. U.S.A. 98*, 10131−10136.
30. Luecke, H., Schobert, B., Lanyi, J. K., Spudich, E. N., and Spudich, J. L. (2001) Crystal structure of sensory rhodopsin II at 2.4 Å: Insights into color tuning and transducer interaction, *Science 293*, 1499−1503.

31. Otomo, J. (1996) Influence exercised by histidine-95 on chloride transport and the photocycle in halorhodopsin, *Biochemistry 35*, 6684−6689.
32. Otomo, J., Tomioka, H., and Sasabe, H. (1992) Properties and the primary structure of a new halorhodopsin from halobacterial strain mex, *Biochim. Biophys. Acta 1112*, 7−12.
33. Soppa, J., Duschl, J., and Oesterhelt, D. (1993) Bacterioopsin, haloopsin, and sensory opsin I of the halobacterial isolate *Halobacterium* sp. strain SG1: Three new members of a growing family, *J. Bacteriol. 175*, 2720−2726.
34. Ihara, K., Umemura, T., Katagiri, I., Kitajima-Ihara, T., Sugiyama, Y., Kimura, Y., and Mukohata, Y. (1999) Evolution of the archaeal rhodopsins: Evolution rate changes by gene duplication and functional differentiation, *J. Mol. Biol. 285*, 163−174.
35. Bivin, D. B., and Stoeckenius, W. (1986) Photoactive retinal pigments in haloalkaliphilic bacteria, *J. Gen. Microbiol. 132*, 2167−2177.
36. Váró, G., Brown, L. S., Sasaki, H., Kandori, H., Maeda, A., Needleman, R., and Lanyi, J. K. (1995) Light-driven chloride ion transport by halorhodopsin from *Natronobacterium pharaonis*. 1. The photochemical cycle, *Biochemistry 34*, 14490−14499.
37. Duschl, A., Lanyi, J. K., and Zimányi, L. (1990) Properties and photochemistry of a halorhodopsin from the haloalkalophile, *Natronobacterium pharaonis*, *J. Biol. Chem. 265*, 1261−1267.
38. Shimono, K., Iwamoto, M., Sumi, M., and Kamo, N. (1997) Functional expression of *pharaonis* phoborhodopsin in *Escherichia coli*, *FEBS Lett. 420*, 54−56.
39. Hohenfeld, I. P., Wegener, A. A., and Engelhard, M. (1999) Purification of histidine tagged bacteriorhodopsin, *pharaonis* halorhodopsin and *pharaonis* sensory rhodopsin II functionally expressed in *Escherichia coli*, *FEBS Lett. 442*, 198−202.
40. Sato, M., Kanamori, T., Kamo, N., Demura, M., and Nitta, K. (2002) Stopped-flow analysis on anion binding to blue-form halorhodopsin from *Natronobacterium pharaonis*: Comparison with the anion-uptake process during the photocycle, *Biochemistry 41*, 2452−2458.
41. Sato, M., Kikukawa, T., Asairo, T., Okita, H., Shimono, K., Kamo, N., Demura, M., and Nitta, K. (2003) Roles of Ser130 and Thr126 in chloride binding and photocycle of *pharaonis* halorhodopsin, *J. Biochem. 134*, 151−158.
42. Scharf, B., and Engelhard, M. (1994) Blue halorhodopsin from *Natronobacterium pharaonis*: Wavelength regulation by anions, *Biochemistry 33*, 6387−6393.
43. Takao, K., Kikukawa, T., Araiso, T., and Kamo, N. (1998) Azide accelerates the decay of M-intermediate of *pharaonis* phoborhodopsin, *Biophys. Chem. 73*, 145−153.
44. Birge, R. R. (1990) Nature of the primary photochemical events in rhodopsin and bacteriorhodopsin, *Biochim. Biophys. Acta 1016*, 293−327.
45. Sato, M., Kikukawa, T., Araiso, T., Okita, H., Shimono, K., Kamo, N., Demura, M., and Nitta, K. (2003) Ser-130 of *Natronobacterium pharaonis* halorhodopsin is important for the chloride binding, *Biophys. Chem. 104*, 209−216.
46. Hasselbacher, C. A., Spudich, J. L., and Dewey, T. G. (1988) Circular dichroism of halorhodopsin: Comparison with bacteriorhodopsin and sensory rhodopsin I, *Biochemistry 27*, 2540−2546.
47. Dencher, N. A., and Heyn, M. P. (1982) Preparation and properties of monomeric bacteriorhodopsin, *Methods Enzymol. 88*, 5−10.
48. Gottschalk, M., Dencher, N. A., and Halle, B. (2001) Microsecond exchange of internal water molecules in bacteriorhodopsin, *J. Mol. Biol. 311*, 605−621.
49. Ogurusu, T., Maeda, A., and Yoshida, T. (1984) Absorption spectral properties of purified halorhodopsin, *J. Biochem. 95*, 1073−1082.
50. Subramaniam, S., and Henderson, R. (2000) Molecular mechanism of vectorial proton translocation by bacteriorhodopsin, *Nature 406*, 653−657.
51. Klare, J. P, Bordignon, E., Engelhard, M., and Steinhoff, H. J. (2004) Sensory rhodopsin II and bacteriorhodopsin: Light activated helix F movement, *Photochem. Photobiol. Sci. 3*, 543−547.
52. Radzwill, N., Gerwert, K., and Steinhoff, H. J. (2001) Time-resolved detection of transient movement of helices F and G in doubly spin-labeled bacteriorhodopsin, *Biophys. J. 80*, 2856−2866.
53. Sass, H. J., Buldt, G., Gessenich, R., Hehn, D., Neff, D., Schlesinger, R., Berendzen, J., and Ormos, P. (2000) Structural alterations for proton translocation in the M state of wild-type bacteriorhodopsin, *Nature 406*, 649−653.
54. Vonck, J. (2000) Structure of the bacteriorhodopsin mutant F219L N intermediate revealed by electron crystallography, *EMBO J. 19*, 2152−2160.
55. Oka, T., Yagi, N., Tokunaga, F., and Kataoka, M. (2002) Time-resolved X-ray diffraction reveals movement of F helix of D96N bacteriorhodopsin during M-MN transition at neutral pH, *Biophys. J. 82*, 2610−2616.
56. Hackmann, C., Guijarro, J., Chizhov, I., Engelhard, M., Rödig, C., and Siebert, F. (2001) Static and time-resolved step-scan Fourier transform infrared investigations of the photoreaction of halorhodopsin from *Natronobacterium pharaonis*: Consequences for models of the anion translocation mechanism, *Biophys. J. 81*, 394−406.

BI047500F